

Demonstrating quantum computing with the quark model

R. M. Woloshyn
TRIUMF, 4004 Wesbrook Mall
Vancouver, British Columbia, V6T 2A3, Canada

Abstract

The use of quantum computing to solve a problem in quantum mechanics is illustrated, step by step, by calculating energies and transition amplitudes in a nonrelativistic quark model. The quantum computations feature the use of variational quantum imaginary time evolution implemented using automatic differentiation to determine ground and excited states of charmonium. The calculation of transition amplitudes is illustrated utilizing the Hadamard test. Examples of readout and gate error mitigation are included

1 Introduction

Nonrelativistic quark models with confining potentials were developed in the 1970's [1, 2, 3]. Doing calculations with these models is a straightforward application of quantum mechanics. In this note the quark model is used to illustrate the steps required to do such calculations on a quantum computer. Often quantum computing examples are drawn from Quantum Chemistry. However, these examples may not be completely understandable without considerable background knowledge of chemistry. On the other hand, the quark model is sufficiently simple that the calculations presented here should be accessible with only a basic knowledge of quantum mechanics.

A quantum computation of quarkonium was presented in [4] using an algorithm different from the one used here. As well, only energies of spin averaged S-wave states were considered. In this work, the spin dependent interaction is included and a P-wave is also calculated. The calculation of transition amplitudes is also discussed.

A feature of the calculations is the use of automatic differentiation in implementing the variational quantum imaginary time evolution [5]. Automatic differentiation software constructs instructions for calculating derivatives of functions themselves defined by software. It is implemented in classical computing libraries such as Autograd [6] and Jax [7] and it is natural that this functionality should be extended to quantum computers. The PennyLane quantum computing

framework [8] has extensive built-in automatic differentiation capability mainly focused on machine learning applications. However, quantum automatic differentiation does have applications in scientific computations [9, 10] and will be used here as it vastly simplifies the use of variational quantum imaginary time evolution.

The steps that will be followed to carry out the quantum computations are enumerated here and will be discussed in subsequent sections.

1. Choose a quark model, *i.e.*, fix the form of the potential and the model parameters.
2. Calculate the matrix elements of the model Hamiltonian in a finite set of basis states. Typically Harmonic oscillator states are used.
3. Rewrite the Hamiltonian matrix in terms of Pauli operators acting on a quantum register, *i.e.*, on a set of qubits.
4. Determine the ground state. Variational quantum imaginary time evolution (VQITE) implemented using automatic differentiation will be used.
5. Determine excited states.
6. Construct the operators that describe transitions between different states, *e.g.* $M1$ and $E1$ transitions between mesonic states with different quantum numbers. The swap test and the Hadamard test will be introduced here.
7. Check the computation on a wave function simulator and on an ideal quantum computer simulator.
8. Check the effect of hardware noise and develop a noise mitigation strategy.
9. Run on real quantum hardware.

It is hoped that this note may be of use to people who are starting to explore quantum computing for scientific applications or to instructors teaching quantum mechanics who would like to introduce quantum computing to their students. It is assumed that the reader has some understanding of qubits, gates, circuits and how to setup and run quantum programs using available quantum computing frameworks but may not yet be very familiar with the common algorithms or applications. For the most part, the PennyLane library [8] was used with Qiskit [11] used for noisy simulations. No code is provided here. In any case, the serious reader would naturally prefer to write her own code.

2 Quark model

2.1 Schrödinger equation

The quark model with confining potentials was developed in the 1970's [1, 2, 3] after the discovery of the J/ψ meson. The version adopted here was used by

α_s	b	m_c	σ
0.5461	0.1425 GeV ²	1.4794 GeV	1.0946 GeV

Table 1: Parameters of the quark model.

Barnes *et al.* [12] in a study of charmonium, that is, mesons composed of a charm quark and an anti-charm quark. Ref. [12] contains an exhaustive study of many high-lying states. For illustrative purposes in this note we restrict the calculation to the mesons η_c , J/ψ and h_c and their excited states. In the usual spectroscopic notation these are the states 1S_0 , 3S_1 and 1P_1 .

The potential takes the form

$$V(r) = -\frac{a}{r} + br + V_s(r)\vec{S}_c \cdot \vec{S}_{\bar{c}},$$

where $a = \frac{4\alpha_s}{3}$ and spin-dependent potential $V_s(r)$ is

$$V_s(r) = \frac{32\pi\alpha_s}{9m_c^2}\delta(r),$$

with $\delta(r) = (\sigma/\sqrt{\pi})^3 e^{-\sigma^2 r^2}$ and m_c is the charm quark mass. Recall that the value of the spin-spin operator $\vec{S}_c \cdot \vec{S}_{\bar{c}}$ is $-\frac{3}{4}$ in singlet states and $\frac{1}{4}$ in triplet states. Note also that the potential contains spin-orbit and tensor terms. They are not relevant for the states we consider and are omitted here. The parameters¹ of the model determined by Barnes *et al.* [12] are given in Table 1.

For a given orbital angular momentum l the radial wave function, written as $u(r) = R(r)/r$ in the notation of Ref. [13], is determined by

$$\left(-\frac{d^2}{2\mu dr^2} + V(r) + \frac{l(l+1)}{2\mu r^2}\right)R(r) = ER(r), \quad (1)$$

where μ is the reduced mass. The meson mass is equal to the energy eigenvalue E plus $2m_c$. There are many options for obtaining the solution of (1). The Schrödinger equation solver `nsolve.f90` [14] was used here. Table 2 contains the energy eigenvalues and masses. There is good agreement with the nonrelativistic model results given in [12].

2.2 Harmonic oscillator basis

The next step in preparing the quark model calculation for a quantum computer is to formulate the problem in matrix form. Choose a finite set of basis states in which to represent the Hamiltonian. The harmonic oscillator wave functions, commonly used in Nuclear Physics [13], are a convenient choice. Like the quark model potential, the oscillator potential is also confining and most of the calculations for matrix elements can be done in closed form.

¹The parameters are quoted as in Barnes *et al.* in GeV units. In the calculation it will be convenient to use the unit fm (fermi or femtometer). Recall the conversion factor $\hbar c = 1 = 197.32$ MeV fm.

1S_0			3S_1		1P_1	
State	E [fm $^{-1}$]	Mass	E [fm $^{-1}$]	Mass	E [fm $^{-1}$]	Mass
1	0.115	2982	0.665	3090	2.826	3516
2	3.403	3630	3.613	3672	4.901	3934
3	5.496	4043	5.640	4072	6.692	4279
4	7.221	4384	7.335	4409	8.418	4585

Table 2: Quark model energy eigenvalues from Eq. (1) in units of fm $^{-1}$ and masses in units of MeV.

The Hamiltonian for the harmonic oscillator in three dimensions is

$$H_{HO} = -\frac{\vec{\nabla}^2}{2\mu} + \frac{1}{2}\mu\omega^2 r^2, \quad (2)$$

so the quark model Hamiltonian can be written as

$$H_{qm} = H_{HO} + V(r) - \frac{1}{2}\mu\omega^2 r^2. \quad (3)$$

Recall that for quantum numbers n, l, m the harmonic oscillator wave function (unnormalized) is

$$r^l e^{-\frac{1}{2}\nu r^2} L_{n+l-1/2}^{l+1/2}(\nu r^2) Y_{lm}(\theta, \phi),$$

where $\nu = \mu\omega$. The eigenenergy is $\omega(2n + l - \frac{1}{2})$ with \hbar set equal to 1. For the present calculation the basis is truncated to four states. The radial integrals needed to calculate the matrix elements of (3) mainly involve powers of r times a Gaussian and can be done analytically. The matrix element of the spin-dependent term can be computed numerically.

The truncated Hamiltonian matrix depends on the oscillator parameter ω . The energy eigenvalues calculated by diagonalizing the Hamiltonian matrix are shown in Fig. 1 as function of ω for the 1S_0 channel. The results in other channels are similar. The dashed lines in the figure are the exact results from solving the Schrödinger equation. The basis truncation introduces an error which, of course, could be reduced by enlarging the basis. For purposes of illustrating the quantum computing process we will proceed with only four states and choose a value of ω equal to 1.2 fm $^{-1}$. The Hamiltonian matrix (in units of fm $^{-1}$) for the 1S_0 channel at this value of ω is

$$\begin{pmatrix} 0.9431 & -0.8733 & -0.7690 & -0.5601 \\ -0.8733 & 3.33652 & -0.5646 & -0.8648 \\ -0.7690 & -0.5646 & 5.4382 & -0.1566 \\ -0.5601 & -0.8648 & -0.1566 & 7.3451 \end{pmatrix}. \quad (4)$$

The matrices for the 3S_1 and 1P_1 channels are given in the Appendix. The eigenvalues E of the Hamiltonian matrices at $\omega = 1.2$ fm $^{-1}$ are in Table 3 and they will be a target of the quantum computation.

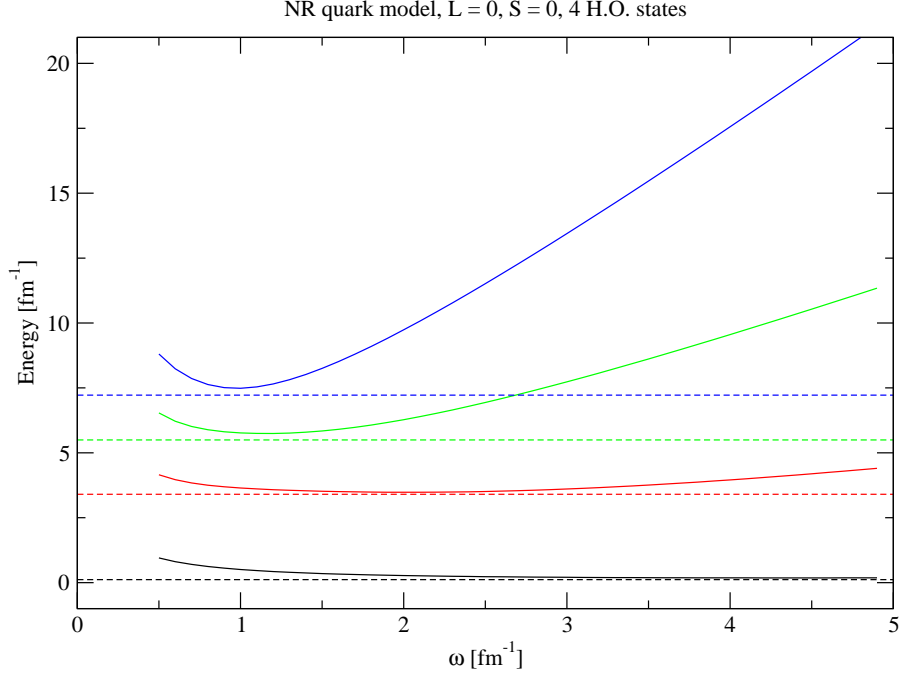


Figure 1: Energy eigenvalues as function of the harmonic oscillator parameter ω for the 1S_0 charmonium states from diagonalizing the Hamiltonian Matrix truncated to four basis states. Dashed lines are results from solving the Schrödinger equation.

2.2.1 Hamiltonian in Pauli form

Four states can be encoded in two qubits and is this is what will be used in the quantum computation. The Hamiltonian matrix is rewritten as the sum of Pauli terms consisting of a coefficient times a product of Pauli operators. In the present case, two operators. In general, the number of operators in a Pauli term equals the number of qubits. Counting the Identity as a Pauli operator the number of possible Pauli terms for n qubits is 4^n or 16 for the present case. Since (4) is a real matrix only ten terms will contribute. The Hamiltonians in Pauli form for the quark model problem are then (omitting Identity operators)

$$c_0 + c_1 Z_0 + c_2 Z_1 + c_3 Z_0 Z_1 + c_4 X_0 + c_5 X_1 + c_6 Z_0 X_1 + c_7 X_0 Z_1 + c_8 X_0 X_1 + c_9 Y_0 Y_1,$$

where the subscripts on the Pauli operators X, Y, Z denote the qubit on which the operator acts. The coefficients for the 1S_0 Hamiltonian Eq. (4) are

$$c = \{4.273, -2.119, -1.082, -0.129, -0.817, -0.515, -0.358, 0.048, -0.562, -0.002\}.$$

	1S_0	3S_1	1P_1
State	E [fm $^{-1}$]	E [fm $^{-1}$]	E [fm $^{-1}$]
1	0.395	0.753	2.783
2	3.506	3.634	4.875
3	5.664	5.723	6.765
4	7.546	7.648	8.767

Table 3: Energy eigenvalues from diagonalizing the truncated Hamiltonian matrices.

The coefficients for 3S_1 are

$$c = \{4.439, -2.122, -1.086, -0.137, -0.655, -0.350, -0.361, 0.044, -0.401, 0.010\},$$

and for 1P_1

$$c = \{5.798, -1.910, -0.964, -0.067, -0.446, 0.083, -0.323, -0.064, -0.095, 0.133\}.$$

3 Variational Quantum Imaginary Time Evolution

There are a number of options available to calculate energy eigenvalues by quantum computation. Quantum phase estimation [15, 16] was developed early on but is considered too demanding for today's limited quantum computing resources. The variational quantum eigensolver [17, 18] is probably the most popular method. There are many variations of this algorithm [19, 20] including schemes for calculating excited states.

In this work we use an alternative, namely, imaginary time evolution. To see why this is useful consider a Hamiltonian H with eigenvalues $\{\lambda_i\}$ and eigenstates $\{|\phi_i\rangle\}$. Then an arbitrary initial state $|\psi_0\rangle$ can be expanded as $\sum_i \langle\phi_i|\psi_0\rangle|\phi_i\rangle$. The action of $e^{-H\tau}$ on $|\psi_0\rangle$ is then

$$e^{-H\tau}|\psi_0\rangle = \sum_i e^{-\lambda_i\tau} \langle\phi_i|\psi_0\rangle|\phi_i\rangle. \quad (5)$$

It is clear that for sufficiently large τ , the lowest-energy eigenstate having an overlap with $|\psi_0\rangle$ will dominate the sum in (5) so that measuring the imaginary time evolution (left hand side of (5)) in that limit will allow a determination of the lowest eigenvalue.

Quantum computing uses unitary operators so the non-unitary operation (5) can not be implemented as written. The key insight is to preserve the norm of the state during evolution. Consider an evolution step $\Delta\tau$. One wants to find a unitary operator $U(\Delta\tau)$ such that

$$|\psi_{\tau+\Delta\tau}\rangle = U(\Delta\tau)|\psi_\tau\rangle = \frac{e^{-H\Delta\tau}|\psi_\tau\rangle}{\sqrt{\langle\psi_\tau|e^{-2H\Delta\tau}|\psi_\tau\rangle}}. \quad (6)$$

At this point, one has options of how to choose the initial state which will also affect how the unitary operator is determined. For example, one can choose a simple to prepare state for $|\psi_0\rangle$, such as a computational basis state. Then, matching a $\Delta\tau$ expansion of different sides of (6) gives equations for an effective unitary operator. This is the strategy of [21, 22]. An attractive feature of this approach is that no commitment is made to the form of the wave function.

An alternative is to use a parametrized variational ansatz for $|\psi_0\rangle$. The evolution will then involve a step-by-step updating of the variational parameters. This is the variational quantum imaginary time evolution of [5] and the method that will be used here.

The variational state $|\psi(\vec{\theta})\rangle$ depends on a set of parameters $\vec{\theta}$ that are implicit functions of τ and is produced by a chosen parametrized unitary operator (the variational ansatz)

$$|\psi(\vec{\theta})\rangle = U(\vec{\theta})|0\rangle.$$

The evolution of $|\psi(\vec{\theta})\rangle$ is governed by the variational principle [5, 23]

$$\delta_{\theta} \left\| (\partial_{\tau} + H - E_{\tau}) |\psi(\vec{\theta}(\tau))\rangle \right\| = 0, \quad (7)$$

where

$$E_{\tau} = \langle \psi(\vec{\theta}(\tau)) | H | \psi(\vec{\theta}(\tau)) \rangle, \quad (8)$$

and δ_{θ} denotes the variation with respect to the parameters $\vec{\theta}$. The derivation of the equations describing the evolution of the variational parameters is given in the Supplementary Information of Ref. [5]. The result is

$$\sum_j A_{ij} \dot{\theta}_j = C_i, \quad (9)$$

with

$$C_i = -\frac{\partial E_{\tau}}{\partial \theta_i}, \quad (10)$$

and

$$A_{ij} = -\frac{\partial^2 \langle \psi(\vec{\theta}) | \psi(\vec{\theta}) \rangle}{\partial \theta_i \partial \theta_j}, \quad (11)$$

where $\bar{\theta}$ is used to indicate that the derivatives in (11) act only on the right hand side of the overlap. After solving (9) for $\dot{\theta}$ the parameters are updated according to $\theta(\tau + \Delta\tau) = \theta(\tau) + \Delta\tau\dot{\theta}$ where $\Delta\tau$ acts like a learning rate parameter.

For the computation done here with four basis states the circuit in Fig. 2 is used for the variational ansatz. With three parameters this circuit can produce any superposition of four states with real coefficients. The circuit used for the overlap in (11) is shown in Fig. 3.

Although one normally associates variational calculations with ground states, the calculation can be extended to excited states as described in [18]. For example, if $|\phi\rangle$ denotes the already determined ground state then adding

$$\alpha \left| \langle \phi | \psi(\vec{\theta}) \rangle \right|^2 \quad (12)$$

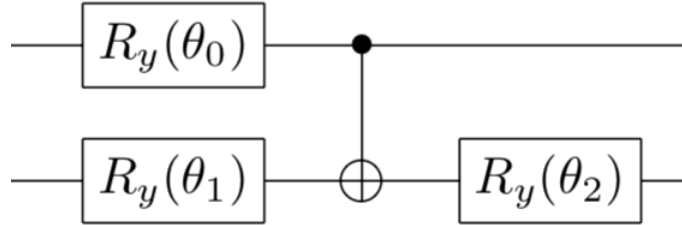


Figure 2: Circuit for the variational wave function encoded in two qubits.

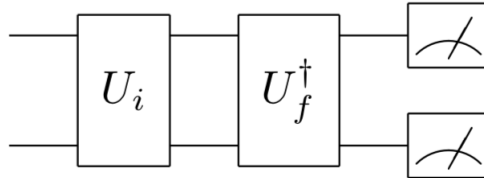


Figure 3: Circuit for the wave function overlap squared $|\langle \psi_f | \psi_i \rangle|^2$ by measuring $U_f^\dagger U_i$.

to the energy (8) with a sufficiently large coefficient α will ensure that the variational calculation will converge to the first excited state. This procedure can then be repeated to get even higher lying states. The circuit in Fig. 3 is used for the overlap.

The PennyLane library is used to carry out the computations. Automatic differentiation of quantum circuits is implemented in this framework so calculating derivatives (10) and (11) is very easy. The PennyLane methods used for (10) and (11) were `pennylane.grad` and `pennylane.gradients.param_shift_hessian` respectively. Note that calculating the gradient in (10) with the energy augmented by (12) does not require any additional work on the programmer's part when automatic differentiation is used.

For the first pass at computing energies the PennyLane `default.qubit` device was used. With shots set equal to `None` this device acts like a wave function simulator, that is, it returns results without quantum measurement uncertainty. This provides a check on the code. With a non-zero number of shots it simulates an ideal quantum computer. The step size was 0.02 and the variational parameters were initialized to be 0.5. Figs. 4, 5 and 6 show how the energies in each channel change as the variational parameters evolve. The horizontal dashed lines are the eigenenergies from diagonalizing the truncated Hamiltonian matrices (see Table 3).

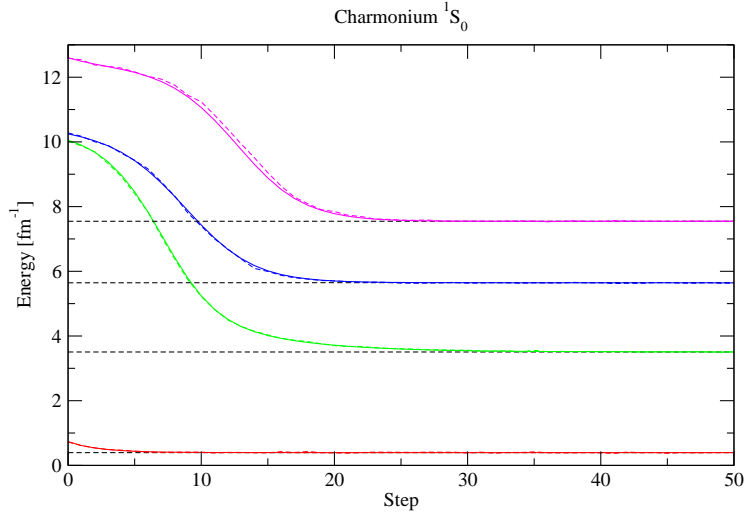


Figure 4: Evolution of the energy as a function of imaginary time step for the 1S_0 channel. The solid lines are results from wave function simulator and the coloured dashed are for an ideal quantum simulation doing 20000 shots per measurement. The horizontal dashed lines are the eigenenergies from diagonalizing the truncated Hamiltonian matrix (4).

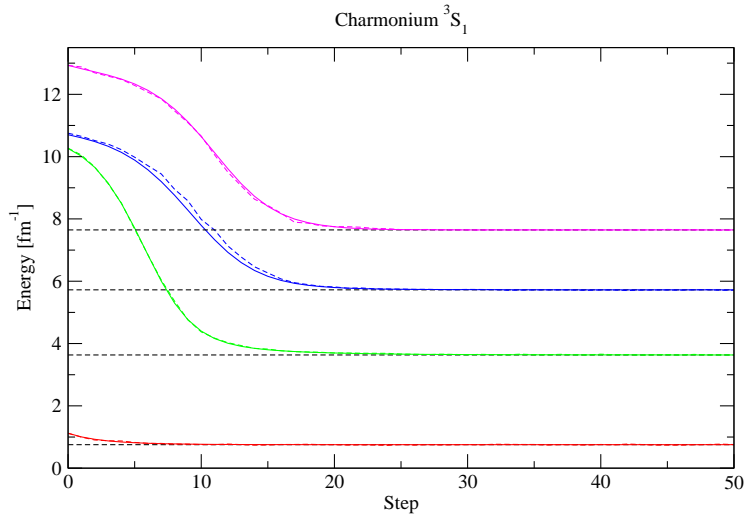


Figure 5: Evolution of the energy as a function of imaginary time step for the 3S_1 channel. The solid lines are results from wave function simulator and the coloured dashed are for an ideal quantum simulation doing 20000 shots per measurement. The horizontal dashed lines are the eigenenergies from diagonalizing the truncated Hamiltonian matrix (15).

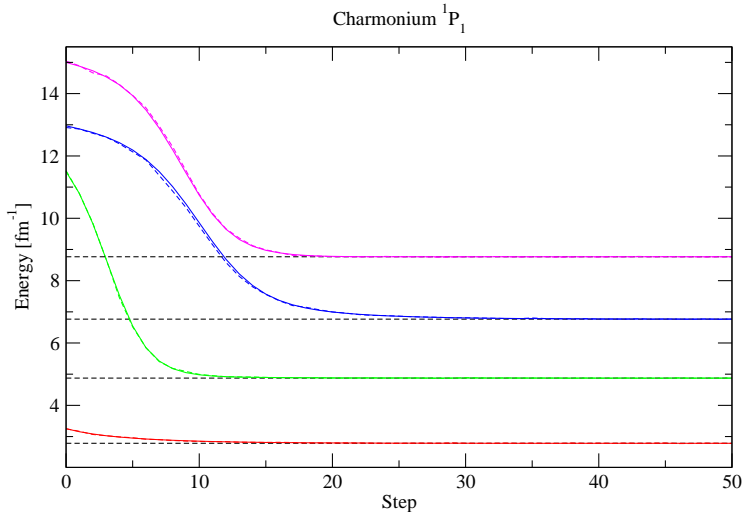


Figure 6: Evolution of the energy as a function of imaginary time step for the 1P_1 channel. The solid lines are results from wave function simulator and the coloured dashed are for an ideal quantum simulation doing 20000 shots per measurement. The horizontal dashed lines are the eigenenergies from diagonalizing the truncated Hamiltonian matrix (16).

4 Transition amplitudes

Having determined variational parameters that yield good ground and excited state energies one can use the wave functions to compute other quantities. Of particular interest for charmonium are $M1$ and $E1$ transition amplitudes. These were discussed in detail by Barnes *et al.* [12].

4.1 M1 transitions

Spin singlet and spin triplet states with the same orbital angular momentum can transform into each other via a spin flip. In the nonrelativistic limit the transition amplitude is just the overlap of the spatial wave functions. Since the quark model Hamiltonian is spin dependent there will be a finite energy transition from the higher energy triplet ground state to the lower energy singlet ground state. Also, there can be excited state to ground state transitions from one spin channel to the other since the spatial wave functions are not orthogonal. Examples of these transitions are considered here

The square of the wave function overlap can be calculated using the $U_i U_f^\dagger$ circuit (Fig. 3) that was used in the variational calculation in Sec. 2. For comparison amplitudes were also calculated using solutions of Eq. (1). These are the exact results of the model and deviations from them will show the effect

Transition	Exact	w.f. sim	$U_i U_f^\dagger$	Swap
$1^3S_1 \rightarrow 1^1S_0$	0.9826	0.9937	0.9939(2)	0.9938(2)
$2^3S_1 \rightarrow 1^1S_0$	0.0107	0.0041	0.0041(1)	0.0035(17)
$2^3S_1 \rightarrow 2^1S_0$	0.9781	0.9935	0.9936(1)	0.9934(2)
$3^3S_1 \rightarrow 2^1S_0$	0.0061	0.0015	0.0016(1)	0.0025(18)
$2^1S_0 \rightarrow 1^3S_1$	0.0123	0.0048	0.0047(1)	0.0045(17)
$3^1S_0 \rightarrow 1^3S_1$	0.0025	0.0011	0.0012(1)	0.0001(14)

Table 4: Squared amplitudes for selected $M1$ transitions. Exact results are calculated using solutions of Eq. (1). The last columns are results from simulation of a ideal quantum computer using circuits in Fig. 3 and 7 respectively.

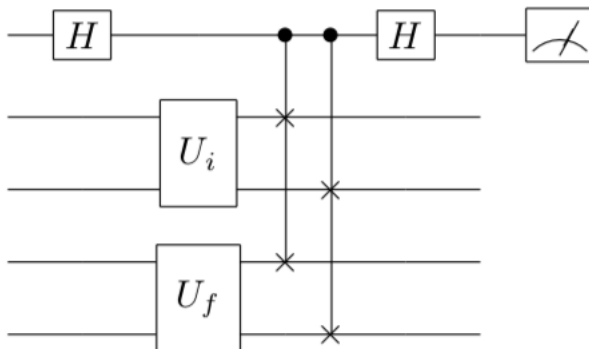


Figure 7: Circuit for the wave function overlap squared $|\langle \psi_f | \psi_i \rangle|^2$ using the swap test.

of the basis truncation.

Results for examples of squared amplitudes for $M1$ transitions are given in Table 4. The values are either very close to one or to zero. This reflects the orthonormality of the eigenstates. The small spin-dependent interaction breaks the degeneracy of the spin-singlet and spin-triplet states and shifts the overlap values slightly away from one and zero.

The column w.f. sim shows results with the PennyLane `default.qubit` device and shots equal to `None`, essentially a wave function simulator. The last two columns are results from simulations of an ideal quantum computer doing 20000 shots per measurement. The results are averaged over twenty trials. With 20000 shots, the $U_i U_f^\dagger$ circuit (Fig. 3) gives excellent agreement with the wave function simulator.

A commonly used algorithm for wave function overlap is the swap test. The circuit is shown in Fig. 7 and the working of the swap test is explained in the Appendix. The result of the measurement in the swap test yields $\frac{1}{2}(1 + |\langle \psi_f | \psi_i \rangle|^2)$ from which the squared overlap can be inferred. This means that when the overlap is small, the uncertainty will be large unless the measurement is

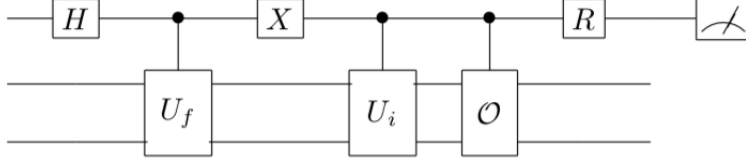


Figure 8: Circuit for calculating the transition amplitude $\langle \psi_f | \mathcal{O} | \psi_i \rangle$ using a Hadamard test. The gate R is $R_y(-\pi/2)$ or $R_x(\pi/2)$ for the real and imaginary parts respectively.

very precise. This is reflected in the results in the last column of Table 4. There are other variations of the swap test, for example, given in [24]. Investigating these is left as an exercise for the reader.

4.2 E1 transitions

States with the same spin and differing by one unit in orbital angular momentum can be connected by E1 transitions. Aside from an angular momentum dependent factor the transition is governed by the spatial matrix element $\langle u_f(r) | r | u_i(r) \rangle$ involving the radial wave functions of the initial and final states [12]. This is the quantity that will be calculated here.

Begin by calculating matrix elements of r between the radial wave functions of the truncated harmonic oscillator basis. For P-wave to S-wave transitions this gives (in units of fm)

$$\begin{pmatrix} 0.57751 & -0.4715 & 0 & 0 \\ 0 & 0.7455 & -0.6668 & 0 \\ 0 & 0 & 5.4382 & -0.9166 \\ 0 & 0 & 0 & 1.0002 \end{pmatrix}. \quad (13)$$

Written in Pauli form (13) becomes

$$\begin{aligned} c_0 + c_1 Z_0 + c_2 Z_1 + c_3 Z_0 Z_1 + c_4 (X_0 X_1 + Y_0 Y_1) + c_5 (X_1 - i Y_1) \\ + c_6 Z_0 (X_1 + i Y_1) + c_7 (X_0 Y_1 - Y_0 X_1), \end{aligned} \quad (14)$$

with coefficients

$$c = \{0.8013, -0.1398, -0.0715, -0.0125, 0.1667, -0.3220, 0.0863, 0.1667i\}.$$

The matrix elements of the Pauli terms in (14) between different states are calculated using a Hadamard test circuit. It is shown in Fig. 8 and its operation is described in the Appendix. The rotation operator R is chosen such that the measurement yields either the expectation value of σ_x or σ_y for the first qubit from which the real or imaginary part of the operator \mathcal{O} matrix element value can be inferred.

Transition	Exact	w.f. sim	1000	10000
$1^1P_1 \rightarrow 1^1S_0$	0.3490	0.3925	0.3929(37)	0.3900(13)
$2^1P_1 \rightarrow 2^1S_0$	0.5900	0.7174	0.7229(42)	0.7172(12)
$2^1S_0 \rightarrow 1^1P_1$	0.5757	0.5406	0.5433(73)	0.5409(24)
$3^1S_0 \rightarrow 2^1P_1$	0.8873	0.8227	0.8174(49)	0.8201(18)
$3^1S_0 \rightarrow 1^1P_1$	0.0311	0.0448	0.0449(65)	0.0448(23)

Table 5: Examples of E1 transition amplitudes. The results in the last two columns were calculated using a Hadamard test circuit with 1000 and 10000 shots per measurement respectively.

The results for the radial matrix elements (in units of fm) for some examples of $E1$ transitions are shown in Table 5. Just as for the $M1$ overlaps, the results calculated with the exact wave functions, i.e., solutions of (1), are also tabulated. The truncated basis calculation reproduces the exact results reasonably well and with 10000 shots per measurement the quantum simulation agrees very well with the wave function simulator results.

5 Noisy simulation

So far only ideal quantum simulations have been considered. The uncertainties that arise are due to the stochastic nature of quantum measurement and they can be reduced by increasing the number of times measurements are carried out. On a real quantum device there will also systematic errors due to noise in the hardware. There can be errors, referred to as gate errors, which affect the unitary operations that the circuit carries out. In addition, qubits may be mis-measured, i.e., readout error.

To get an idea of how a computation may be affected by hardware noise one can introduce a noise model in the quantum simulator. The Qiskit framework is very useful for doing this since it provides noise models based on actual IBM quantum hardware as well as a capability of creating custom noise models. It also provides some tools for mitigating or correcting hardware errors. PennyLane, which is the framework used in this work, has cross-platform capability through the use of plug-ins, so that we can include Qiskit resources within our code.

As a first example the mitigation of readout errors in the calculations of energies is considered. Results for the 1^1S_0 channel are shown here, Figs 9, 10 and 11. Results for the other channels should be similar. The noise model used is for the device `ibmq_manila`. After downloading the noise model² a calibration run is done to determine the readout fidelity of the qubits that will be measured in the actual calculations. When the calculations are done the calibration matrix is applied to the measurement before the computing final

²An IBM Quantum account is needed to download the noise model. An alternative which does not need an account is to use a fake device, eg., FakeManila, which is included in the Qiskit software.

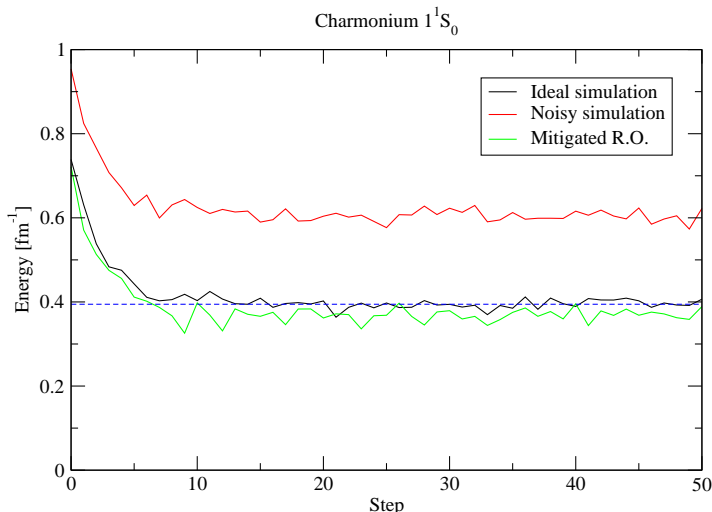


Figure 9: Evolution of the energy as a function of imaginary time step for the 1^1S_0 ground state. Results of ideal, noisy and readout error mitigated simulations are shown. The horizontal dashed line is the eigenenergy from diagonalizing the truncated Hamiltonian matrix (16).

results. The procedure used here is described in [25]. Note that for illustration purposes, only readout error was included in the noise model. Mitigating gate errors when using automatic differentiation [10] goes beyond the scope of this pedagogical note.

The next example is the effect of readout error on the wave function squared overlaps that govern $M1$ transitions. Results, calculated using the circuit in Fig. 3, are in Table 6.

The effects of readout error are substantial. For the large overlaps, mitigating readout errors brings the results close to the ideal noise-free results. When the overlap is small, mitigating the read out error provides an improvement but not enough to provide a reliable estimate of the true noise-free value.

Transition	No noise	With R.O. error	Mitigated
$1^3S_1 \rightarrow 1^1S_0$	0.9939(2)	0.9385(1)	0.9813(1)
$2^3S_1 \rightarrow 1^1S_0$	0.0041(1)	0.0596(1)	0.0320(1)
$2^3S_1 \rightarrow 2^1S_0$	0.9936(1)	0.9386(1)	0.9808(1)
$3^3S_1 \rightarrow 2^1S_0$	0.0016(1)	0.0270(1)	0.0036(1)
$2^1S_0 \rightarrow 1^3S_1$	0.0047(1)	0.0614(1)	0.0327(1)
$3^1S_0 \rightarrow 1^3S_1$	0.0012(1)	0.0526(1)	0.00008(4)

Table 6: Calculations of squared amplitudes for selected $M1$ transitions showing the effect of readout error and mitigation.

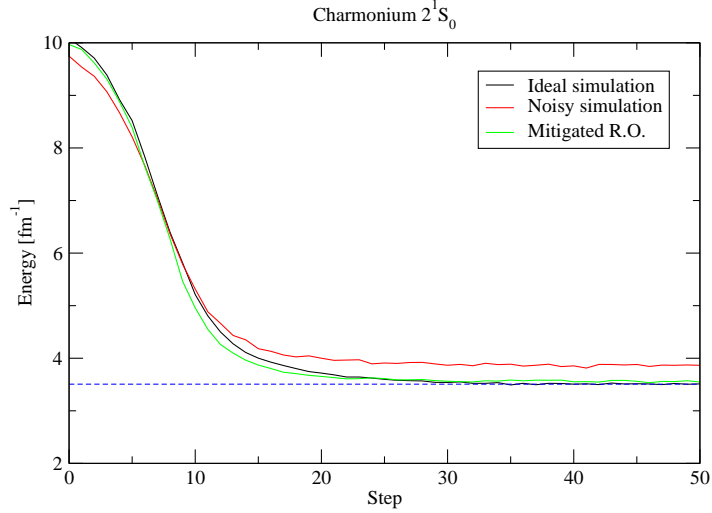


Figure 10: Evolution of the energy as a function of imaginary time step for the 1S_0 first excited state. Results of ideal, noisy and readout error mitigated simulations are shown. The horizontal dashed line is the eigenenergy from diagonalizing the truncated Hamiltonian matrix (4).

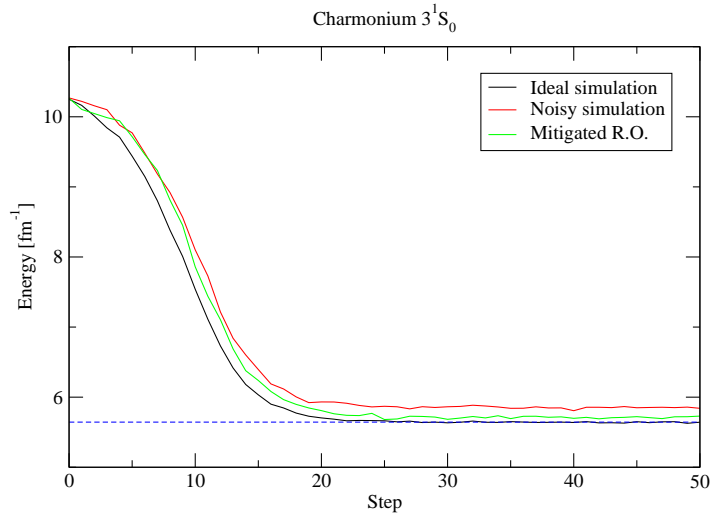


Figure 11: Evolution of the energy as a function of imaginary time step for the 1S_0 second excited state. Results of ideal, noisy and readout error mitigated simulations are shown. The horizontal dashed line is the eigenenergy from diagonalizing the truncated Hamiltonian matrix (4).

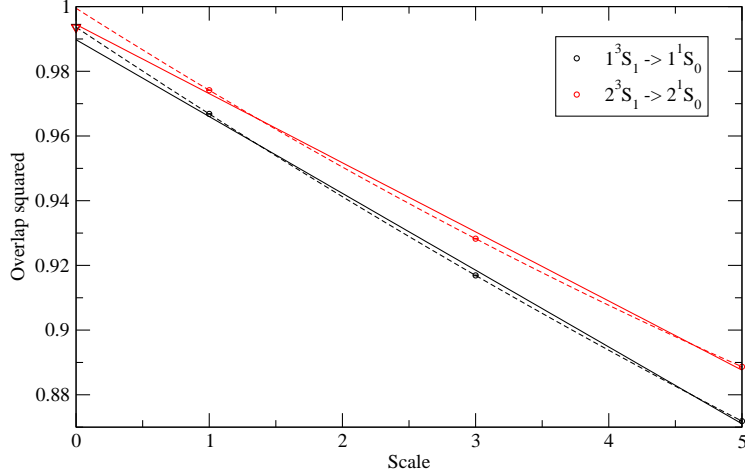


Figure 12: Wave function overlap squared for selected $M1$ transitions having a large amplitude as function of circuit unitary folding scale. The solid and dashed lines are linear and second-order polynomial zero-noise extrapolations. The results of noise-free simulations are shown by triangles at scale equal 0.

There are many suggestions of how to mitigate gate errors and it is still an active research area [26, 27, 28, 29, 30, 31]. One of the first proposals was the use of zero-noise extrapolation. The general idea is to calculate results with gate noise artificially increased and then extrapolate the results down to zero noise. One way to implement this scheme is so-called unitary folding. Let \mathcal{U} denote the circuit to which gate error mitigation is to be applied. Then the circuits $\mathcal{U}\mathcal{U}^\dagger\mathcal{U}$, $\mathcal{U}\mathcal{U}^\dagger\mathcal{U}\mathcal{U}^\dagger\mathcal{U}$, etc. will have increased gate errors although they would give identical results on an ideal noise-free quantum device. Results with different levels of $\mathcal{U}^\dagger\mathcal{U}$ insertions can be extrapolated to estimate a noise-free value. This scheme was implemented for selected $M1$ transitions calculated using the circuit Fig. 3. The results are shown in the Fig. 12 and 13. Both linear and second-order polynomial extrapolations were used. However, for the transitions in Fig. 13 second-order polynomial extrapolation led to unphysical, *i.e.*, negative values, at zero noise so that extrapolation is omitted. Scale equal 1 means calculation with no unitary folding, scale equal 3 means an insertion of the circuit and its adjoint and so on.

The final example will be gate error mitigation for the swap test circuit Fig. 7. Generally multi-qubit gates are more susceptible to errors than single qubit gates so one would expect that the swap test circuit will have much bigger errors than the circuit in Fig. 3. On a noisy device it will only be feasible to calculate the transitions with amplitude near one. An example of mitigation of gate errors by zero noise extrapolation in a calculation using the swap test circuit is shown in Fig. 14. The effect of gate errors is very large compared to Fig. 12

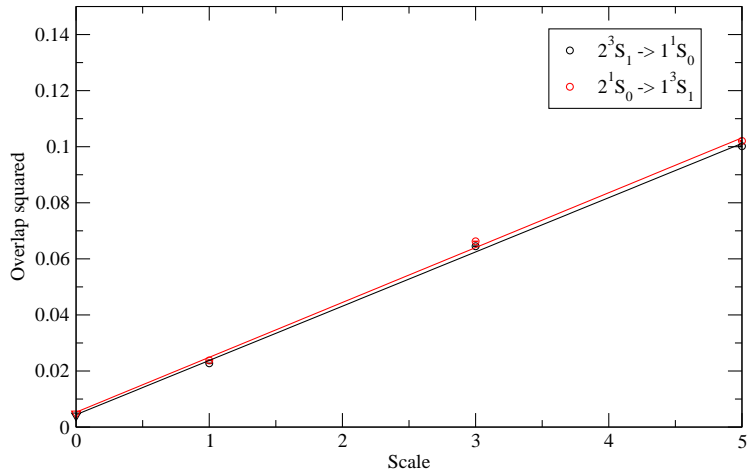


Figure 13: Wave function overlap squared for selected $M1$ transitions having a small amplitude as function of circuit unitary folding scale. The solid lines are linear zero-noise extrapolations. The results of noise-free simulations are shown by triangles at scale equal 0.

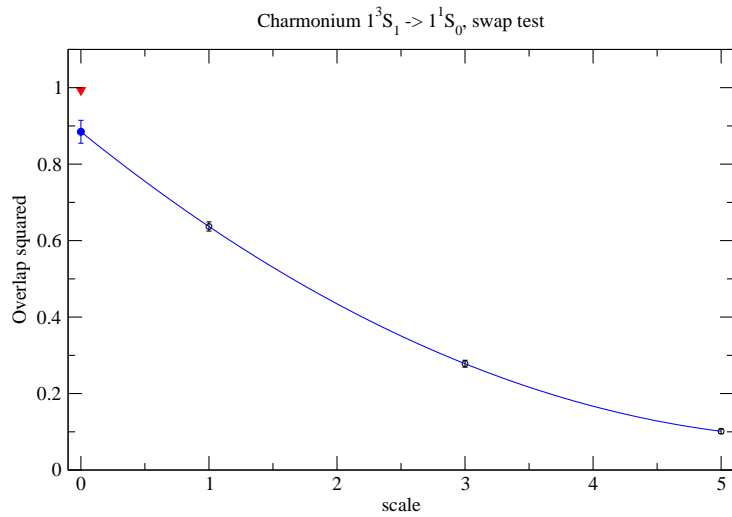


Figure 14: Wave function overlap squared describing the spin-triplet to spin-singlet $M1$ transition as a function of unitary folding scale. The line is a second-order polynomial extrapolation. The result of a noise-free simulation is shown by the triangle at scale equal 0.

Transition	Noise-free simulation	Simulated ibmq_manila	Real ibmq_manila
$1^3S_1 \rightarrow 1^1S_0$	0.9939(2)	0.9414(2)	0.9314(97)
$2^3S_1 \rightarrow 1^1S_0$	0.0041(1)	0.0432(1)	0.0522(40)
$2^3S_1 \rightarrow 2^1S_0$	0.9936(1)	0.9470(1)	0.9253(118)
$3^3S_1 \rightarrow 2^1S_0$	0.0016(1)	0.0223(1)	0.0253(17)
$2^1S_0 \rightarrow 1^3S_1$	0.0047(1)	0.0459(1)	0.0509(37)
$3^1S_0 \rightarrow 1^3S_1$	0.0012(1)	0.0542(1)	0.0640(48)

Table 7: Squared amplitudes for selected $M1$ transitions comparing results obtained on the real `ibmq_manila` device with noise-free and noisy simulations.

where the overlap circuit Fig. 3 was used. Nonetheless, an extrapolation can be made which gets considerably closer to , but not quite in agreement with, the noise-free value. The uncertainty in the extrapolated value was obtained using a bootstrap procedure.

Error mitigation of $E1$ transition amplitudes is left for the reader.

6 Quantum hardware

For completeness, an example of a computations done on a real quantum device will be given in this section. The PennyLane software library was used in this work so using the PennyLane-qiskit plugin allows code to be run on IBM Quantum hardware by setting the PennyLane device to be `qiskit.ibmq` with backend specified as the IBM Quantum device.

In the previous section use was made of the `ibmq_manila` noise model running on a quantum simulator. The first example will be to compare the real `ibmq_manila` device with the simulated one. Since the author’s access to quantum resources is limited, the comparison will be made for the simplest calculation. *i.e.*, wave function overlap squared using circuit Fig. 3.

Squared amplitudes for selected $M1$ transitions calculated without error mitigation on the `ibmq_manila` device are shown in the last column of Table 7. Results are averaged over ten trials doing 20000 shots per measurement. For comparison the results from an ideal noise-free simulation and from simulated results using the `ibmq_manila` noise model are also included. The noisy simulation and real hardware results are similar. The main difference being the larger uncertainty in the hardware results reflecting considerable fluctuation in results of different trails carried out over a period of a few days.

The final example is a calculation of the wave function overlap squared describing the $2^3S_1 \rightarrow 2^1S_0$ transition doing both readout and gate error mitigation. The computed results using different unitary foldings are indicated by open circles in Fig. 15. The solid circle is the zero-noise extrapolated value with uncertainty obtained by a bootstrap analysis.

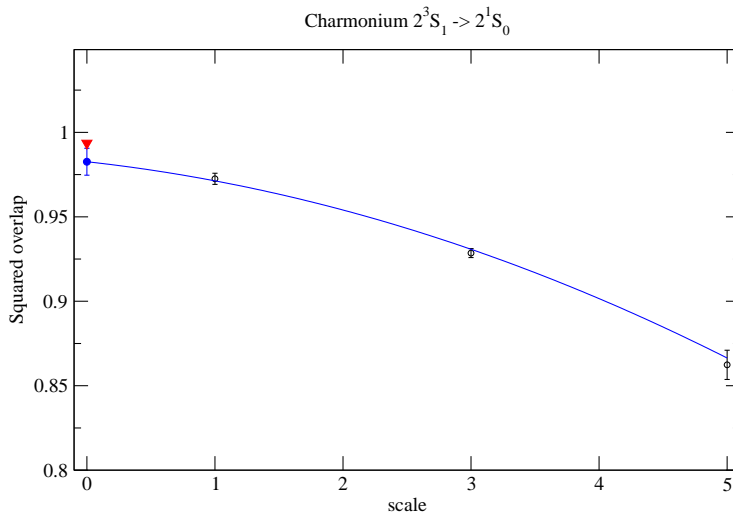


Figure 15: Wave function overlap squared describing the $2^3S_1 \rightarrow 2^1S_0$ transition as a function of unitary folding scale. The line is a second-order polynomial extrapolation. The result of a noise-free simulation is shown by the triangle at scale equal 0.

7 Summary

The calculation of energies and transition amplitudes in a nonrelativistic quark model is used to demonstrate the steps required to carry out quantum computations. Ground and excited states energies of charmonium were calculated using variational quantum imaginary time evolution. The algorithm was implemented using automatic differentiation within the PennyLane quantum computing framework. Amplitudes for selected $M1$ and $E1$ transitions were calculated illustrating the use of the swap test and the Hadamard test.

Effects of readout and gate errors were investigated through the use of simulations with noise models accessed using the Qiskit framework. Readout error correction and zero-noise extrapolation were shown to improve results but in cases, for example, where the transition amplitude was very small error mitigation was not sufficient to yield reliable results.

Some examples of computations carried out on the IBM `ibmq_manila` device were presented. It should be noted that with PennyLane’s cross-platform capability these calculations can be ported easily to other kinds of quantum computing hardware.

Acknowledgement

Thanks to Olivia Di Matteo and Billy Jones for their helpful comments. We acknowledge the use of the IBM Quantum services for this work. The views

expressed are those of the author, and do not reflect the official policy or position of IBM or the IBM Quantum team. TRIUMF receives federal funding via a contribution agreement with the National Research Council of Canada.

Appendix

A.1 Oscillator basis Hamiltonians

The truncated Hamiltonian for 3S_1 at $\omega = 1.2 \text{ fm}^{-1}$

$$\begin{pmatrix} 1.0946 & -0.7114 & -0.6111 & -0.4112 \\ -0.7114 & 3.5406 & -0.3910 & -0.6989 \\ -0.6111 & -0.3910 & 5.6122 & -0.0119 \\ -0.4112 & -0.6989 & -0.0119 & 7.5104 \end{pmatrix}, \quad (15)$$

and for 1P_1

$$\begin{pmatrix} 2.8561 & -0.2395 & -0.3827 & -0.2282 \\ -0.2395 & 4.919 & -0.0373 & -0.5097 \\ -0.3827 & -0.0373 & 6.8114 & 0.4058 \\ -0.2282 & -0.5097 & 0.4058 & 7.5104 \end{pmatrix}. \quad (16)$$

The matrix elements are in units of fm^{-1} .

A.2 Overlap circuits

The swap test and Hadamard test circuits for calculating the transition amplitudes are shown in Figs. 7 and 8. A brief explanation of how these circuits work is given here.

First, consider the swap test. The quantum registers for the ancillary qubit and the initial and final wave functions are initially in the state $|0\rangle_0 |0\rangle_1 |0\rangle_2$ and then operations as listed below are carried out.

Operation	State
	$ 0\rangle_0 0\rangle_1 0\rangle_2$
Hadamard(0)	$\frac{1}{\sqrt{2}} (0\rangle_0 0\rangle_1 0\rangle_2 + 1\rangle_0 0\rangle_1 0\rangle_2)$
$U_i(1)$	$\frac{1}{\sqrt{2}} (0\rangle_0 i\rangle_1 0\rangle_2 + 1\rangle_0 i\rangle_1 0\rangle_2)$
$U_f(2)$	$\frac{1}{\sqrt{2}} (0\rangle_0 i\rangle_1 f\rangle_2 + 1\rangle_0 i\rangle_1 f\rangle_2)$
Controlled Swap(0 : 1 \longleftrightarrow 2)	$\frac{1}{\sqrt{2}} (0\rangle_0 i\rangle_1 f\rangle_2 + 1\rangle_0 f\rangle_1 i\rangle_2)$
Hadamard(0)	$\frac{1}{2} \{ 0\rangle_0 (i\rangle_1 f\rangle_2 + f\rangle_1 i\rangle_2) + 1\rangle_0 (i\rangle_1 f\rangle_2 - f\rangle_1 i\rangle_2) \}$

Now measure the ancillary qubit, register 0. The probability of measuring this qubit in the state $|0\rangle$ is

$$\begin{aligned} P(0) &= \frac{1}{4} (\langle i|_1 \langle f|_2 + \langle f|_1 \langle i|_2) (|i\rangle_1 |f\rangle_2 + |f\rangle_1 |i\rangle_2), \\ &= \frac{1}{2} (1 + \langle i|f\rangle \langle f|i\rangle), \end{aligned}$$

which yields the squared overlap.

The operation of the Hadamard test used to calculate transition amplitudes is described here. The register 0 is an ancillary qubit and the unitary operators describing the states and the transition operator \mathcal{O} act on register 1.

Operation	State
	$ 0\rangle_0 0\rangle_1$
Hadamard(0)	$\frac{1}{\sqrt{2}} (0\rangle_0 0\rangle_1 + 1\rangle_0 0\rangle_1)$
Controlled $U_f(0, 1)$	$\frac{1}{\sqrt{2}} (0\rangle_0 0\rangle_1 + 1\rangle_0 f\rangle_1)$
PauliX(0)	$\frac{1}{\sqrt{2}} (0\rangle_0 f\rangle_1 + 1\rangle_0 0\rangle_1)$
Controlled $U_i(0, 1)$	$\frac{1}{\sqrt{2}} (0\rangle_0 f\rangle_1 + 1\rangle_0 i\rangle_1)$
Controlled $\mathcal{O}(0, 1)$	$\frac{1}{\sqrt{2}} (0\rangle_0 f\rangle_1 + 1\rangle_0 \mathcal{O} i\rangle_1)$

Let $|\psi\rangle$ denote the state $\frac{1}{\sqrt{2}} (|0\rangle_0 |f\rangle_1 + |1\rangle_0 \mathcal{O} |i\rangle_1)$. Then

$$\langle \psi | \sigma_x(0) | \psi \rangle = \frac{1}{2} (\langle f | \mathcal{O} | i \rangle + \langle i | \mathcal{O} | f \rangle),$$

and

$$\langle \psi | \sigma_y(0) | \psi \rangle = -\frac{i}{2} (\langle f | \mathcal{O} | i \rangle - \langle i | \mathcal{O} | f \rangle).$$

References

- [1] E. Eichten *et al.*, Phys. Rev. Lett. **34**, 369 (1975).
- [2] B. J. Harrington, S. Y. Park and A. Yildiz, Phys. Rev. Lett. **34**, 706 (1975).
- [3] E. Eichten, K. Gottfried, T. Kinoshita, K. D. Lane and T. M. Yan, Phys. Rev. D **17**, 3090 (1978).
- [4] D. Gallimore and J. Liao, Quantum computing for heavy quarkonium spectroscopy, [arXiv:2202.03333].
- [5] S. McArdle *et al.*, npj Quantum Information **5** (2019).

- [6] D. Maclaurin, D. Duvenaud and R. P. Adams, Autograd: Effortless gradients in numpy, in *ICML 2015 AutoML Workshop*, 2015.
- [7] J. Bradbury *et al.*, JAX: composable transformations of Python+NumPy programs, <http://github.com/google/jax>, 2018.
- [8] V. Bergholm *et al.*, PennyLane: Automatic differentiation of hybrid quantum-classical computations, [arXiv:1811.04968].
- [9] J. M. Arrazola *et al.*, Differentiable quantum computational chemistry with PennyLane, 2021, [arXiv:2111.09967].
- [10] O. Di Matteo and R. M. Woloshyn, *Phys. Rev. A* **106**, 052429 (2022).
- [11] M. S. ANIS *et al.*, Qiskit: An open-source framework for quantum computing, doi:10.5281/zenodo.2573505.
- [12] T. Barnes, S. Godfrey and E. S. Swanson, *Phys. Rev. D* **72**, 054026 (2005).
- [13] R. R. Roy and B. P. Nigam, *Nuclear Physics* (John Wiley & Sons, 1967).
- [14] <https://github.com/cngilbreth/nsolve>.
- [15] A. Y. Kitaev, Quantum measurements and the abelian stabilizer problem, [arXiv:9511026].
- [16] D. S. Abrams and S. Lloyd, *Phys. Rev. Lett.* **83**, 5162 (1999).
- [17] A. Peruzzo *et al.*, *Nature Communications* **5** (2014).
- [18] T. Jones, S. Endo, S. McArdle, X. Yuan and S. C. Benjamin, *Phys. Rev. A* **99**, 062304 (2019).
- [19] K. M. Nakanishi, K. Mitarai and K. Fujii, *Phys. Rev. Research* **1**, 033062 (2019).
- [20] Y. Ibe *et al.*, *Phys. Rev. Research* **4**, 013173 (2022).
- [21] M. Motta *et al.*, *Nature Physics* **16**, 205 (2019).
- [22] N. Gomes *et al.*, *Journal of Chemical Theory and Computation* **16**, 6256 (2020).
- [23] J. Broeckhove, L. Lathouwers, E. Kesteloot and P. Van Leuven, *Chemical Physics Letters* **149**, 547 (1988).
- [24] L. Cincio, Y. Subaşı, A. T. Sornborger and P. J. Coles, *New Journal of Physics* **20**, 113022 (2018).
- [25] https://qiskit.org/documentation/stable/0.34/tutorials/noise/3_measurement_error_mitigation.html.
- [26] Y. Li and S. C. Benjamin, *Phys. Rev. X* **7**, 021050 (2017).

- [27] M. Krebsbach, B. Trauzettel and A. Calzona, Optimization of Richardson extrapolation for quantum error mitigation, [arXiv:2201.08080].
- [28] S. A Rahman, R. Lewis, E. Mendicelli and S. Powell, Phys. Rev. D **106**, 074502 (2022).
- [29] R. LaRose *et al.*, Quantum **6**, 774 (2022).
- [30] R. LaRose, A. Mari, V. Russo, D. Strano and W. J. Zeng, Error mitigation increases the effective quantum volume of quantum computers, [arXiv:2203.05489].
- [31] E. v. d. Berg *et al.*, Single-shot error mitigation by coherent pauli checks, [arXiv:2212.03937].